Title: Intracellular pH differentially regulates transcription of metabolic and signaling pathways in normal epithelial cells

Authors and Affiliations:
Ricardo Romero-Moreno[1,2], Jessamine F. Kuehn[1,2], Katharine A. White*[1,2]

[1]Harper Cancer Research Institute, South Bend. IN, 46617, USA
[2]Department of Chemistry and Biochemistry, University of Notre Dame, Notre Dame, IN, 46556, USA

Contact Info:

Correspondence: kwhite6@nd.edu

Keywords: Intra cellular pH, pHi, metabolism, glycolysis, Notch signaling

Summary (150 words, currently 148):

Intracellular pH (pHi) dynamics regulate normal cell functions while dysregulated pHi dynamics have been linked to disease. However, the molecular mechanisms linking pHi dynamics and cell biology are poorly understood. Here, we found that just 24 hours of altered pHi can trigger global transcriptional changes in normal human breast epithelial cells, particularly in signaling and metabolic pathways. We identified 176 genes that were differentially expressed with altered pHi, including Notch1 signaling and glycolytic pathway members. We confirmed pH-dependent expression of lactate dehydrogenase and pyruvate dehydrogenase kinase at the protein level and showed this produced a shift toward glycolytic metabolism at high pHi. We also found pH-dependent Notch1 expression and protein abundance, leading to increased downstream Notch1 signaling at high pHi. This work suggests transient pHi dynamics transcriptionally regulate signaling and metabolic pathways, identifies molecular targets driving pH dependent biology, and suggests pathways by which dysregulated pHi may drive disease.

Introduction

Normal epithelial cells have an intracellular pH (pHi) of ~7.2, but transient pHi dynamics (6.8-7.6) have been shown to regulate cell behaviors including cell migration (Denker and Barber, 2002), proliferation (Putney and Barber, 2003), and differentiation (Ulmschneider *et al.*, 2016) (Figure 1A). Transient pHi dynamics are driven by the activity of ion transport proteins including monocarboxylate transporters (De Saedeleer *et al.*, 2014), sodium bicarbonate transporters (Gorbatenko *et al.*, 2014), V-ATPases (Stransky, Cotter and Forgac, 2016), the Na^+-H^+ exchanger 1 (NHE1) (Putney, Denker and Barber, 2002), and anion exchangers (Gorbatenko *et al.*, 2014). At the molecular scale, pH-dependent biology is mediated by proteins or pathways that are sensitive to small, physiological increases (7.2-7.6) or decreases in pHi (6.8-7.2) (Schönichen *et al.*, 2013). The subclass of proteins with activities, abundances, or binding affinities that are sensitive to physiological changes in pHi are called pH sensors.

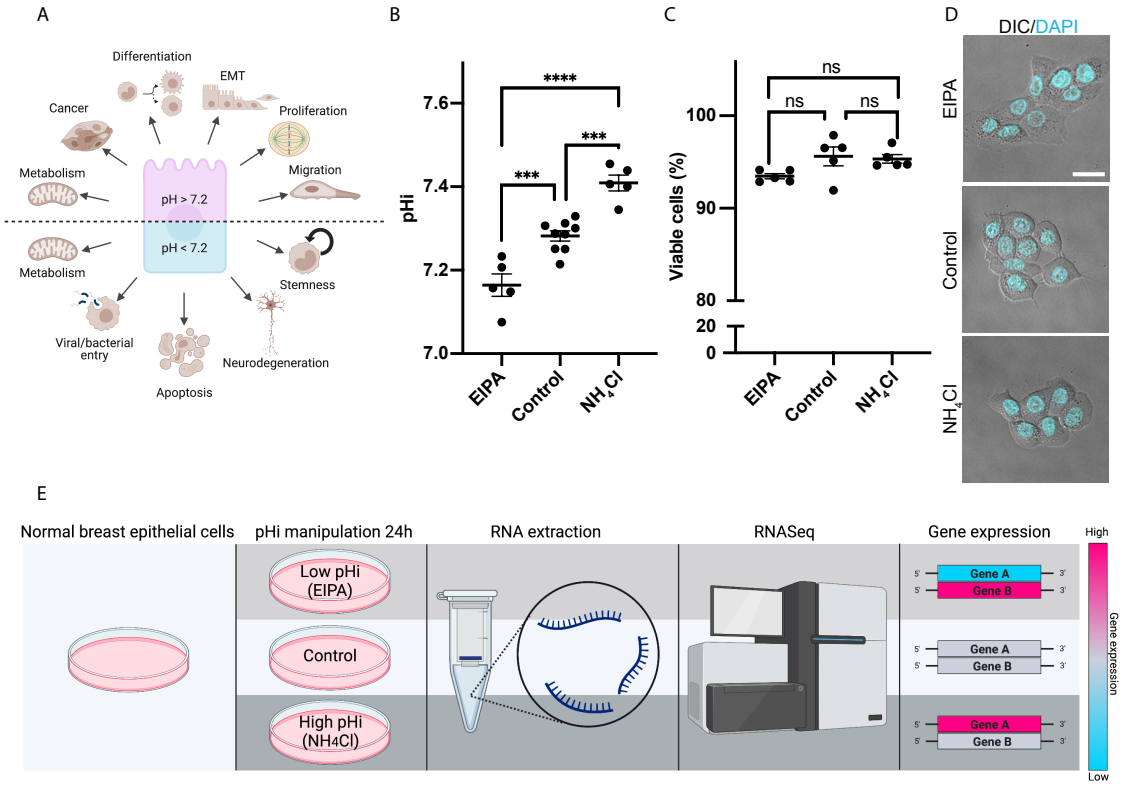

Figure 1. Increasing and decreasing pHi in normal breast epithelial cells does not alter viability or morphology. A) Schematic showing pHi-dependent biology and dysregulated pHi of cancer and neurodegeneration. B) Measured pHi (see methods) in normal human mammary epithelial cells (MCF10A) that were left untreated (control) or treated for 24 hours with complete media containing 25 μM EIPA (EIPA) to lower pHi or 30 mM NH_4Cl (NH_4Cl) to raise pHi. Scatter plot (mean±SEM) from 5-9 biological replicates. C) Trypan blue exclusion assay to assess viability of cells treated as in B. Scatter plot (mean±SEM) from 5 biological replicates. D) Representative confocal images of MCF10A cells treated as in (B). Differential interference contrast (DIC), with overlay of Hoechst dye nuclear stain (DAPI). Scale bars: 20 μm. E) Schematic of pHi manipulation, RNA isolation, and analysis workflow. Resulting RNASeq analysis can identify genes that are upregulated (magenta) or downregulated (cyan) compared to control MCF10A cells. For B and C, significance was determined using ANOVA with Tukey's multiple comparisons correction, ***$p<0.001$, ****$p<0.0001$.

Work identifying pH sensors and pH-sensitive pathways has generally started from the biological outcome, identified a pH-sensitive pathway involved in that process, and then isolated essential proteins in the pathway and tested pH sensitivity of those proteins one by one. This laborious approach has demonstrated successes with the identification of actin cytoskeleton as a pH-sensitive pathway in dictyostelium in 1996 (Stoeckelhuber *et al.*, 1996), mammalian cells in 2006 (Lázaro-Diéguez *et al.*, 2006), and finally the identification of four pH-sensitive proteins involved in actin cytoskeleton remodeling (talin (Srivastava *et al.*, 2008), cofilin (Frantz *et al.*, 2008), cdc42 (Frantz *et al.*, 2007), and focal adhesion kinase (Choi *et al.*, 2013) with full molecular mechanisms characterized.

However, for many pH-sensitive behaviors such as cell-cycle progression (Putney and Barber, 2003), metabolic reprogramming (Benej *et al.*, 2020; Man *et al.*, 2022), and differentiation (Ulmschneider *et al.*, 2016) no mediating pH sensors have been identified. To better understand

the role of pHi in driving epithelial biology, new approaches are needed to rapidly identify pH-dependent proteins or pH-sensitive pathway nodes. With the goal of identifying global pH-dependent transcriptional regulation, work by Putney *et al.*, used a normal mouse fibroblast cell line where a key pH homeostatic regulator (NHE1) was deleted. This cell line was then supplemented with either wild-type NHE1 (LAPN, normal pHi 7.35) or a transport-dead NHE1 variant (E266I) (LAPE, decreased pHi 7.16) (Putney and Barber, 2004). The authors showed that these two cell models had significantly altered expression profiles of transcripts related to cell cycle regulation, growth, and metabolic adaptation (Putney and Barber, 2004).

While this older dataset established a role for intracellular pH in the regulation of normal cell functions via transcriptional regulation, there are four significant limitations. First, Putney *et al.* used a mouse fibroblast cell line, which does not replicate normal human epithelial biology. Second, Putney *et al.* only compared low pHi to normal pHi, whereas most pH-dependent processes with unknown molecular drivers involve transient increases in pHi (e.g., epithelial to mesenchymal transition, cell differentiation, proliferation) (Putney and Barber, 2003; Amith, Wilkinson and Fliegel, 2016; Ulmschneider *et al.*, 2016). Third, Putney *et al.* used an Affymetrix microarray, which has limited transcriptome coverage compared to modern NextGen RNASeq approaches. Finally, Putney *et al.* used genetic manipulation and clonal selection to generate two mouse fibroblast cell lines with normal pHi homeostasis and low pHi homeostasis. Thus, long-term compensatory effects could be a major driver of the identified transcriptional changes that were attributed to pH-dependent transcription. To fully understand pH-dependent mechanisms driving normal human epithelial cell biology, we sought to reveal global transcriptomic regulation of epithelial cells during transient, physiological changes in pHi.

Here, we developed an experimental platform to globally identify pH-dependent transcriptional regulation in normal breast epithelial cells (MCF10A). This project expands upon previous work by using small molecule approaches to both transiently increase (7.41) and decrease (7.16) pHi of normal human mammary epithelial cells (7.28). This approach prevents compensatory responses to altered pHi resulting from genetic ablation of ion transporters and long-term selection, while better recapitulating the transient pHi changes that drive normal cell behaviors. We show that changes in pHi for 24 hours trigger a global change in gene expression profiles. After identifying a subset of transcripts that are differentially regulated at high and low pHi, we biochemically validated a collection of hits in metabolic and signaling pathways. We show that higher pHi transcriptionally upregulates key metabolic enzymes regulating pyruvate fate. We also show for the first time that the Notch signaling pathway, which is highly conserved in development, is differentially regulated by pHi with increased expression and activity at increased pHi when compared to control or the low pHi condition. This work has implications for understanding transcriptional responses of mammalian cells to dynamic changes in pHi and identifies novel pH-dependent pathways and signaling nodes that may underly normal pH-dependent cell physiology and drive dysregulated behaviors in diseases associated with altered pHi dynamics (White, Grillo-Hill and Barber, 2017).

Results

Transient pHi changes in normal mammary epithelial cells do not affect cell viability
The overarching goal of this project is to better understand the role of transient pHi changes in transcriptional regulation of normal mammary epithelial cells. We first identified culture conditions to experimentally raise and lower pHi in normal epithelial cells over 24 hours. We developed an experimental platform where immortalized normal mammary epithelial cells (MCF10A) with a pHi of 7.28±0.01 were treated for 24 hours with 25 μM 5-(N-ethyl-N-isopropyl) amiloride (EIPA), a selective inhibitor of the plasma membrane Na^+-H^+ exchanger NHE1, to significantly decrease pHi to 7.16±0.03 (Figure 1B). Parental MCF10A cells could also be treated for 24 hours with 30 mM ammonium chloride (NH_4Cl) to significantly increase pHi to 7.41±0.02 (Figure 1B). These data show we can experimentally decrease pHi of normal epithelial cells into the physiological range observed during hypoxia (Reshkin, Greco and Cardone, 2014) and maintenance of the adult and embryonic stem cell niche (Ulmschneider *et al.*, 2016) (6.9-7.3). Similarly, we can experimentally increase the pHi of normal cells into the physiological range observed during cell proliferation (Andersen *et al.*, 2016), migration (Denker and Barber, 2002), and metabolic reprogramming (Alfarouk *et al.*, 2020; Czowski *et al.*, 2020).

Because cytosolic acidification below 7.0 has been associated with apoptosis (Lagadic-Gossmann, Huc and Lecureur, 2004), we next assessed cell viability under the pHi-altering conditions using a trypan blue exclusion assay. We avoided redox-dependent viability assays such as CellTiter Blue (Fields and Lancaster, 1993) and mitochondrial activity-based assays (Mosmann, 1983) since these readouts are sensitive to both metabolic and redox activity changes that may be pHi-dependent (Persi *et al.*, 2018; Zhao *et al.*, 2019). There was no significant difference in cell viability between control MCF10A cells and cells with decreased (EIPA) or increased pHi (NH_4Cl) under these treatment conditions (Figure 1C). Additionally, we did not observe significant morphological abnormalities or changes in MCF10A epithelial colony formation when cultured at low or high pHi (Figure 1D). These results suggest that 24-hour treatment with pH manipulation culture conditions does not significantly alter the viability or morphology of MCF10A cells.

Transient changes in pHi alter gene expression profiles in normal mammary epithelial cells
We next characterized the pH-dependent transcriptional profiles of normal MCF10A cells in response to short-term changes in pHi (24 h). We prepared control MCF10A cells and cells treated for 24 hours with the pHi manipulation culture conditions described above. We collected RNA from six independent biological replicates per treatment condition, prepared RNASeq libraries, and performed NextGen RNASeq to identify pH-dependent transcriptional profiles (Figure 1E). All RNASeq transcript data were analyzed in comparison to control, with fold-change averaged across the 6 biological replicates (Supplemental Table 1, see Figure S1 for Principal Component Analysis and clustering of biological replicates). For these combined datasets, fold-change (in log_2) cutoffs were used for upregulation ($log_2FC > 0.5$) and downregulation ($log_2FC < -0.5$) along with a false discovery rate (FDR) cutoff (FDR < 0.05) for both conditions when compared to control.

We generated volcano plots of transcripts at low pHi (Figure 2A) and high pHi (Figure 2B), where grey dots indicate transcripts with significant upregulation ($log_2FC > 0.5$) or downregulation ($log_2FC < -0.5$) compared to control with an FDR < 0.05. We found that low pHi (EIPA) produced 8,660 significantly altered transcripts (4,340 upregulated, 4,320 downregulated) while high pHi (NH_4Cl) produced 3,529 significantly altered transcripts (1,891 upregulated, 1,638 downregulated) compared to control MCF10A (Figure 2C, Supplemental Table 2). Furthermore, we found 176 transcripts exhibited differential expression at low and high

pHi (Figure 2C and Figure S2). Of the 176 transcripts with differential expression, 53 transcripts were upregulated at low pHi and downregulated at high pHi while 123 transcripts were downregulated at low pHi and upregulated at high pHi (Figure 2C and Figure S2). Complete list of differentially regulated genes, fold changes, and significance can be found in Supplemental Table 3. These data suggest that transient changes in pHi (24 h) can trigger global transcriptional changes in MCF10A cells when compared to the control.

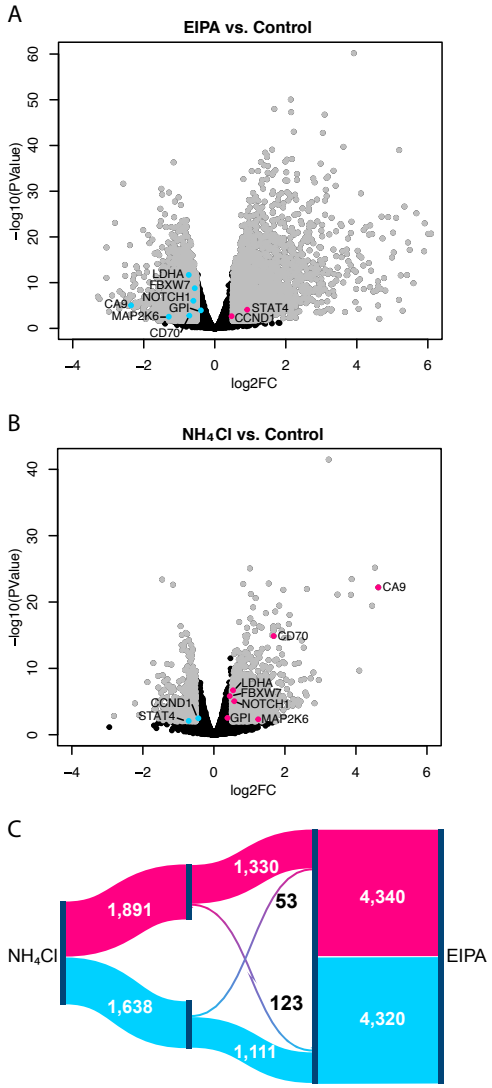

Figure 2. Transient changes in pHi lead to differentially expressed genes in normal epithelial cells. A-B) Volcano plots of RNASeq datasets collected from normal MCF10A cells treated for 24 hours with (A) EIPA to lower pHi or (B) NH_4Cl to raise pHi. Shown in grey are transcripts that are upregulated ($log_2FC > 0.5$, FDR < 0.05) and downregulated ($log_2FC < -0.5$, FDR < 0.5) compared to control. Labeled are a subset of the identified transcripts that are differentially regulated at high and low pHi (magenta upregulated, cyan downregulated). C) Sankey diagram showing all significantly altered transcripts from A-B. 176 genes are differentially regulated at high and low pHi, with 53 genes upregulated (magenta) at low pHi and downregulated (cyan) at high pHi and 123 genes downregulated at low pHi and upregulated at high pHi.

We next compared our RNASeq analysis to the prior microarray dataset obtained from NHE1-null (low pHi) and NHE1-competent (normal pHi) mouse fibroblasts (Putney and Barber, 2004). Overall, from the 193 genes reported in the Putney microarray dataset, 73 (37.8%) were also found in our dataset of significant gene regulation at low pHi compared to control (Figure S3A, Supplemental Table 4). Further analysis revealed that of the 73 common genes, 45 (61.6%) had matched transcriptional regulation in both datasets (Figure S3A, Supplemental Table 4), indicating relatively high directionality concordance of the pH-sensitive transcripts. However, there were some notable differences between the Putney dataset and our dataset, with 28 genes (38.3%) having mismatched gene regulatory effects (Figure S3A, Supplemental Table 4). For example, the key glycolytic enzymes pyruvate kinase muscle isoform (PKM) and hexokinase 2 (HK2) and the cell cycle regulator Wee1 were found to be upregulated at low pHi compared to normal pHi in Putney's mouse fibroblast microarray dataset. However, our RNASeq analysis showed downregulation of these three genes at low pHi compared to normal. This lack of concordance may suggest that cellular context matters (i.e. human epithelial cells vs. mouse fibroblasts) for a subset of pHi-dependent transcripts. Alternatively, the Putney dataset may reflect both pH-dependent effects as well as compensatory transcriptional effects from genetic ablation, clonal selection, and adaptation. These compensatory effects would not be present under the short-term pHi manipulation approaches we used to more closely mimic the physiological dynamics found in normal epithelial cells.

Additionally, Putney *et al.* used their microarray data to build a visual representation of the most relevant gene ontology terms represented in their dataset (Putney and Barber, 2004). Interestingly, many of the identified pathways in their study have been shown to have a pH-dependent behavior such as cell cycle (Putney and Barber, 2003), carbohydrate metabolism (Persi *et al.*, 2018; Alfarouk *et al.*, 2020), ion transporters (Putney, Denker and Barber, 2002), and cell adhesion (Choi *et al.*, 2013). Gene ontology analysis of our RNASeq dataset indicates that signaling (16%) and metabolic pathways (16%) are the two most predominantly altered pathway categories in the pHi-dependent RNASeq dataset (Figure S3B). Taken together, these analyses suggest that transient changes in pHi (24 h) are sufficient to trigger pH-dependent transcriptional regulation in MCF10A and that regulation is clustering in pathways linked to pHi-dependent processes (metabolism and proliferation).

We predicted that genes with differential regulation at high pHi compared to low pHi would be more likely to indicate a true pH-sensitive node and not an off-target effect of treatment. We found that differentially-regulated transcripts included pH-homeostasis regulators (Carbonic anhydrase IX, CA9), metabolic proteins (glucose-6-phosphate isomerase, GPI/G6PI; lactate dehydrogenase, LDHA), cell cycle proteins (cyclin D1, CCND1), signaling receptors and transcriptional activators (Notch homolog 1, NOTCH1; Signal transducer and activator of transcription 4, STAT4), kinases (MAP kinase kinase 6, MAP2K6), and proteasome pathway members (F-box/WD repeat-containing protein 7, FBXW7) (Figure 2A, B). For a complete list of differentially regulated genes see Figure S2 and Supplemental Table 3. We next identified cellular pathways with a high incidence of differentially regulated genes using MetaCore pathway analysis software (Clarivate Analytics, see methods) and found that transcription of glycolytic and Notch 1 pathway enzymes was generally increased at high pHi and decreased at low pHi compared to control MCF10A.

Glycolytic pathway enzymes are upregulated at high pHi and downregulated at low pHi
Data is conflicting on the role for pHi in altering metabolism. Some data suggest pHi is a driver of metabolic changes (Putney and Barber, 2004; Persi *et al.*, 2018) while others suggest altered pHi is a response to metabolic changes (Druzhkova *et al.*, 2016). Our data suggest that transcription of glycolytic pathway enzymes is generally increased at high pHi and decreased at

low pHi compared to control (Figure 3A). Additionally, prior computational analyses has suggested that glycolytic flux may be increased at high pHi and that low pHi may inhibit glycolysis (Persi *et al.*, 2018). While the Persi *et al.* computational analysis was performed on the predicted activity of glycolytic enzymes, these results and our RNASeq data both suggest that reversible (such as glucose-6-phosphate isomerase and triosephosphate isomerase) and irreversible enzymes (such as hexokinase and pyruvate kinase) are affected by pHi (Supplemental Table 5). Taken together this suggests that transient changes in pHi may be a sufficient driver of metabolic reprogramming in normal epithelial cells. Furthermore, the predicted activity of the metabolic enzymes in combination with our analysis of mRNA transcript abundance may suggest that transcription and activity work concomitantly to regulate metabolism in a pH-dependent manner.

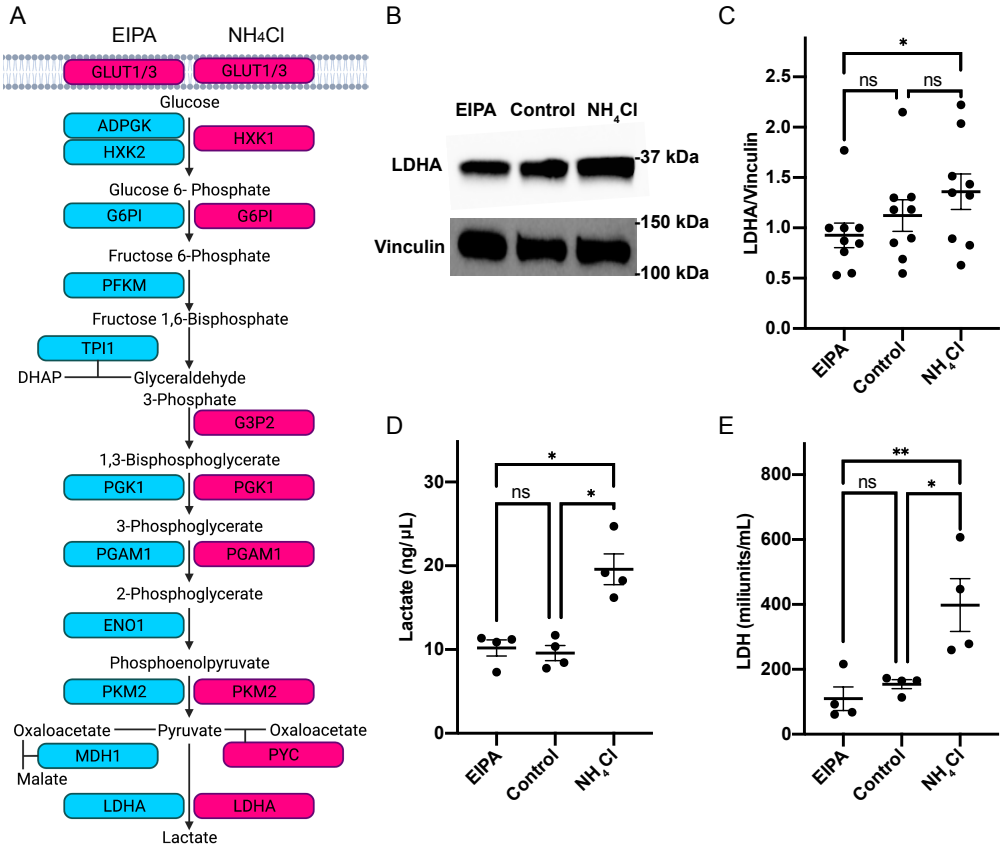

Figure 3. High pHi favors a glycolytic metabolism through increased expression and function of glycolytic enzymes. A) Glycolytic pathway genes with transcripts that were upregulated (magenta) or downregulated (cyan) at low pHi (EIPA, left) or high pHi (NH_4Cl, right) compared to the control. (MetaCore pathway analysis; see methods). B) Representative immunoblot for lactate dehydrogenase A (LDHA) and loading control (vinculin) using lysates from control MCF10A cells or MCF10A cells treated for 24 hours with EIPA to lower pHi or NH_4Cl to raise pHi (see methods for details). C) Quantification of immunoblots prepared as in B. LDHA expression was normalized to vinculin loading control. Scatter plot (mean ±SEM) from 9 biological replicates. D) Measurement of intracellular lactate (see methods) in cells treated as in B. Scatter plot (mean±SEM) from 4 biological replicates. E) Measurement of lactate dehydrogenase activity in lysates of cells treated as in B. Scatter plot (mean±SEM) from 4 biological replicates. For C,D, and E significance was determined using ANOVA with Tukey's multiple comparisons correction; *$p<0.05$, **$p<0.01$.

While our data suggest that high pHi increases glycolytic flux, one key determinant of metabolic reprogramming is the fate of pyruvate inside cells. For oxidative metabolism, pyruvate is primarily processed through pyruvate dehydrogenase (PDH) to generate Acetyl-CoA (AcCoA) for citric acid cycling, while a shift to proliferative (glycolytic) metabolism is marked by conversion of pyruvate to lactate via lactate dehydrogenase A (LDHA). Our RNASeq analysis found pHi-dependent transcription of several enzymes regulating pyruvate fate. In MCF10A cells, LDHA is differentially regulated by pHi, with upregulation at high pHi and downregulation at low pHi compared to control (Figure 3A). Importantly, while LDHA has previously been shown to be downregulated at low pHi (Putney and Barber, 2004) matching our observations, our data also suggests that high pHi upregulates LDHA expression compared to control cells. In addition to the transcriptional regulation of LDHA, we also found a novel role for pHi in regulating expression of pyruvate dehydrogenase kinase (PDK1) which phosphorylates the E1 subunit of PDH to negatively regulate activity and reduce conversion of pyruvate to AcCoA. PDK1 expression is upregulated at high pHi and downregulated at low pHi (Supplementary Table 3). This suggests that high pHi could increase PDK1-dependent inhibition of PDH and reduce conversion of pyruvate into AcCoA while simultaneously enhancing LDHA and conversion of pyruvate to lactate. Taken together, these data suggest higher pHi inhibits oxidative phosphorylation and could lead to a more glycolytic metabolism while low pHi favors decreased PDK1 expression, activation of PDH, and high conversion of pyruvate into AcCoA for entry into the Krebs cycle during cellular respiration.

LDHA protein expression and activity are upregulated at high pHi compared to low pHi
Protein abundance does not always correlate with transcript levels, and many glycolytic enzymes are highly allosterically regulated. Thus, we biochemically confirmed observed pH-dependent transcriptional changes in LDHA using assays for protein abundance and activity. There was a trend of higher LDHA protein abundance in MCF10A at higher pHi, with significant increases in abundance at high pHi compared to low pHi (Figure 3B, C). Single-cell immunofluorescent staining also showed that LDHA protein was significantly increased at high pHi and significantly decreased at low pHi compared to control MCF10A (Supplemental Figure 4A, B). These results confirm that the observed changes in LDHA transcription produced altered protein abundance, with increased LDHA abundance at high pHi and reduced abundance at low pHi at both the population and single-cell levels.

We next conducted two functional assays of LDHA activity in MCF10A. First, we measured the concentration of intracellular lactate in control MCF10A cells compared to MCF10A cells with high and low pHi. We found cellular lactate levels were significantly increased at high pHi when compared to both the control and the low pHi conditions, however no difference was found between control and low pHi (Figure 3D). We also measured activity of LDH from lysates isolated from control MCF10A cells and MCF10A cells at high and low pHi. We found that the LDH isolated from cells with high pHi was more active than the LDH isolated from cells with control or low pHi (Figure 3E). Taken together, these results suggest that changes in pHi can significantly alter the glycolytic pathway at the transcriptional, protein, and functional levels. Additionally, these results support prior work showing that LDHA activity increases with increased pHi (Read *et al.*, 2001) suggesting that changes in LDHA transcription and activity both support changes in cellular metabolism.

We next assessed whether transcriptional changes in PDK1 altered PDK1 protein abundance. We found that PDK1 abundance was increased at high pHi compared to low pHi and decreased at low pHi compared to control (Figure S5A, B). Immunofluorescent imaging also showed that PDK1 protein was significantly increased in single cells at high pHi when compared to control and low pHi MCF10A cells (Figure S5C, D). Together these data suggest that increased pHi

could produce a more glycolytic metabolism by not only increasing the conversion of pyruvate to lactate, but also reducing conversion of lactate to AcCoA via regulation of PDH activity by PDHK.

NOTCH signaling pathway is upregulated at high pHi and downregulated at low pHi
We used MetaCore pathway analysis to construct a Notch1 signaling pathway based on the RNASeq transcriptional data. Transcripts for many NOTCH1 pathway members are differentially regulated by pHi (Figure 2A, B). While NOTCH1 has never been reported to have a pH-dependent abundance or function, some studies have shown that decreased activity of Notch1 pathway members are associated with stem cell maintenance (Blanpain *et al.*, 2006; Micchelli and Perrimon, 2006) while upregulation of Notch1 signaling is linked to cell commitment to differentiation (Bouras *et al.*, 2008; He and Zou, 2019). Stem cell maintenance and differentiation processes have been previously shown to have pH-dependent regulation, with low pHi required to maintain the stem cell niche and high pHi being necessary for differentiation (Ulmschneider *et al.*, 2016). However, despite being associated with these pH-dependent behaviors, Notch1 expression and activity has not been shown to be pH-sensitive.

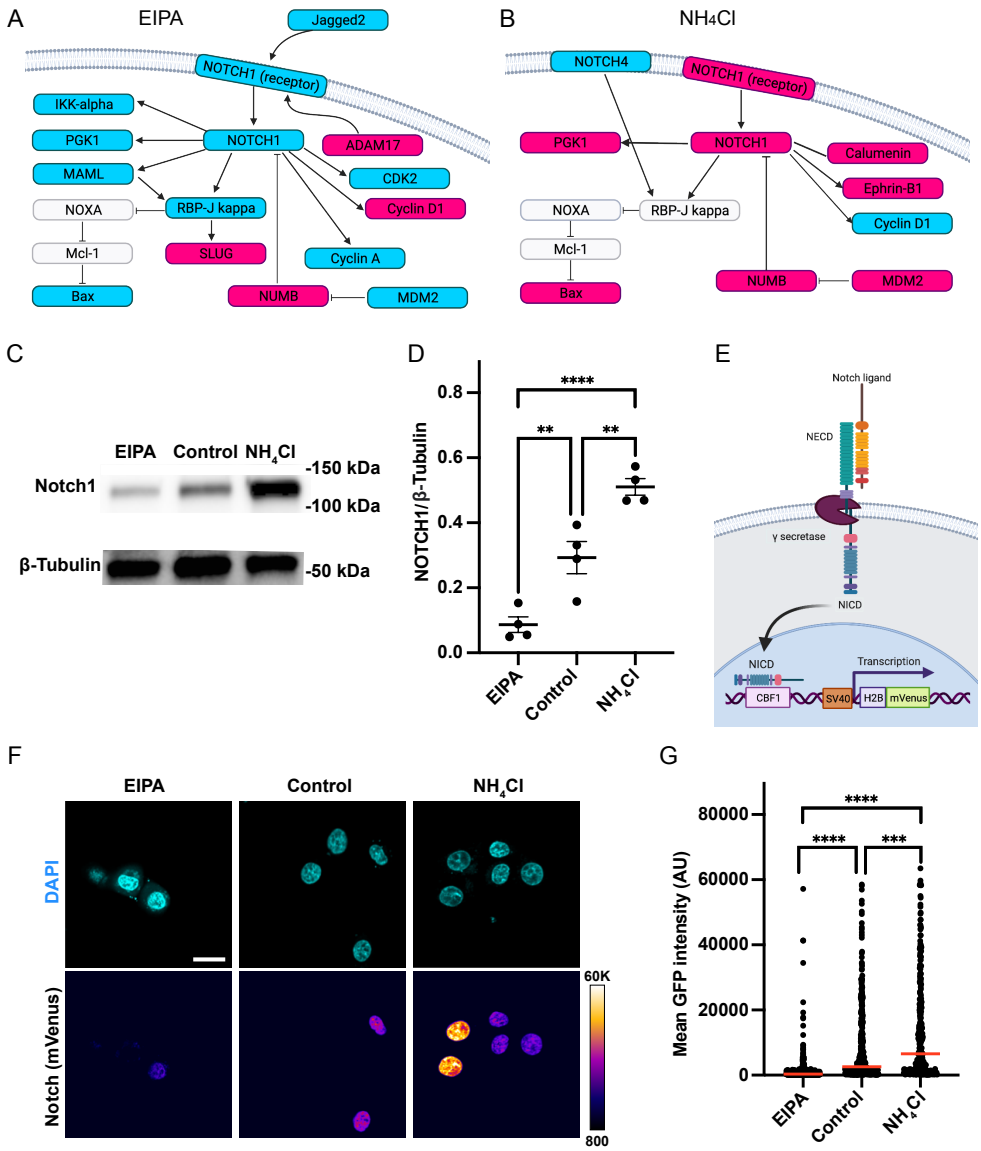

Figure 4. High pHi increases Notch1 expression and signaling activity and low pHi decreases expression and signaling. A-B) Notch1 signaling pathway genes with transcripts that are upregulated (magenta) or downregulated (cyan) at low pHi (EIPA) (A) or high pHi (NH_4Cl). (B) compared to the control. (Metacore pathway analysis; see methods). C) Representative immunoblot for Notch1 and loading control (tubulin) using lysates from control MCF10A cells or MCF10A cells treated for 24 hours with EIPA to lower pHi or NH_4Cl to raise pHi (see methods for details). D) Quantification of immunoblots prepared as in C. Notch1 expression was normalized to tubulin loading control. Scatter plot (mean±SEM) from 4 biological replicates. E) Schematic Notch1 signaling reporter used to quantify Notch1 activity in single-cells. Binding of Notch1 to CBF promoter drives mVenus fluorescent protein expression. F) Representative confocal images of MCF10A cells expressing the Notch1 activity reporter and treated as in C. Notch1 reporter fluorescence is shown in intensiometric display and nuclei were stained with Hoechst dye (DAPI). Scale bars: 20 μm G) Quantification of Notch reporter activity from images collected as in F. Reporter fluorescence intensity from individual cell nuclei are shown in scatter plot (mean±SEM) from 3 biological replicates. For D, significance determined using ANOVA with Tukey's multiple comparisons correction. For G, significance determined

using Kruskal-Wallis with Dunn's multiple comparisons correction; **p<0.01, ***p<0.001, ****p<0.0001.

NOTCH1 itself is differentially regulated in the RNASeq data (Figure 2A, B; Figure 4A, B). At low pHi NOTCH1 is downregulated, along with several downstream targets of Notch1 signaling pathway like PGK1, CyclinA, and CDK2, CBF1, MAML, and IKK alpha (Figure 4A). At high pHi Notch1 is upregulated, along with several downstream targets of Notch1 signaling pathway like PGK1, Calumenin, Ephrin-B1 (Figure 4B). Interestingly we observed that NUMB, a negative regulator of the Notch1 pathway, is upregulated at both high and low pHi which was surprising. However, MDM2, a negative regulator of NUMB, is differentially regulated with high expression at high pHi and low expression at low pHi. Notch1 is a unique signaling molecule in that there is a lack of an amplification step during signal transduction (Andersson, Sandberg and Lendahl, 2011). Thus, Notch expression changes generally correlate strongly with signal output. Given this pathway result, we predicted that Notch1 pathway activity would be lower at low pHi and higher at high pHi.

We next sought to biochemically validate pH-dependent changes in Notch1 protein abundance and downstream pathway activation. Notch1 protein abundance in cell lysates was increased at high pHi and decreased at low pHi when compared to control MCF10A cells (Figure 4C, D). To assay for pH-dependent Notch1 pathway activation, we used a Notch1 signaling reporter (Nowotschin *et al.*, 2013) where nuclear mVenus expression is driven under a CBF1 promoter (Figure 4E). We transfected a large pool of MCF10A cells with the reporter then plated cells in triplicate on imaging dishes for 24 hours to recover. The transfected MCF10A cells were then treated with EIPA (low pHi), NH_4Cl (high pHi), or left untreated (control) for 24 hours before Notch reporter activity was assessed in single cells using confocal microscopy (Figure 4F). We observed that Notch signaling activity was increased at high pHi and decreased at low pHi compared to control (Figure 4G). Together, these data suggest that pHi-dependent changes in Notch transcript and protein abundance can produce pHi-dependent increases in Notch1 pathway activation.

In summary, these RNASeq analyses show that normal mammary epithelial cells exhibit pH-dependent transcription of Notch1 pathway members involved in cell cycle, metabolism, apoptosis, and proteostasis. Our biochemical and cell biological analyses show that Notch1 protein abundance is pH-dependent, leading to pH-dependent Notch1 activity. The Notch signaling pathway is an evolutionarily conserved pathway that has been well characterized for its roles in cellular and tissue development, differentiation, angiogenesis, and proliferation (Wang *et al.*, 2006; Siekmann and Lawson, 2007; Andersson, Sandberg and Lendahl, 2011). And while it has been previously shown that Notch1 signaling is a highly regulated process, including regulation by environmental factors such as temperature (Nomura *et al.*, 2022), this is the first evidence suggesting a role for pHi in regulating Notch1 expression and signaling activity.

Discussion

Transient changes in pHi are known to enable normal cell behaviors, but in most cases the molecular mechanisms and essential pH-sensitive pathways are not known. Here, we provide evidence that pHi dynamics can drive global transcriptional changes in just 24 hours in normal epithelial cells. Our results improve on a previous dataset (Putney and Barber, 2004) by using human epithelial cells, increasing transcriptome coverage, and achieving higher specificity of pHi manipulation with reduced cellular adaptation effects. We identified 176 transcripts that are differentially regulated at high pHi compared to low pHi, suggesting pHi can function as a

rheostat in regulating gene transcription. Pathway analysis showed that the top 500 gene ontology (GO) processes affected by changes in pHi were metabolism (84, 16%) and signaling/signal transduction (83, 16%) followed by differentiation, biosynthesis, and cell cycle (with less than 50 GO terms each). This suggests a potential role for pHi-dependent transcription in regulating these pathways. We also validated the role for pHi in driving expression changes in key pathway hubs in the Notch1 signaling pathway (Notch1) and clarify the role for pHi in regulating expression of metabolic pathway enzymes (LDHA and PDK1).

The pH-dependent transcriptome characterized in this study will have value for epithelial biologists as well as biologists and biochemists working in cancer and neurodegeneration as constitutively increased pHi is a common feature of cancer (Damaghi, Wojtkowiak and Gillies, 2013; White, Kisor and Barber, 2019; Czowski *et al.*, 2020), while decreased pHi is linked to neurodegenerative diseases (Chaumeil *et al.*, 2012; Ruffin *et al.*, 2014). Increased pHi in cancer has been shown to enable cancer cell behaviors such as increased proliferation (Putney and Barber, 2003), metastasis (Amith, Wilkinson and Fliegel, 2016), and evasion from apoptosis (Perez-Sala, Collado-Escobar and Mollinedo, 1995). However, very little is known about whether increased pHi is sufficient to drive tumorigenic phenotypes in human epithelial cells.

Metabolic reprogramming has been linked to various normal pH-dependent processes including stem cell differentiation (Tsogtbaatar *et al.*, 2020), epithelial to mesenchymal transition (EMT) (Kang *et al.*, 2019), and cell migration (Bhattacharya, Azambuja and Simoes-Costa, 2020; Mosier *et al.*, 2021). However, it is not known whether metabolic changes drive pHi dynamics or whether pHi dynamics drive metabolic changes in these processes. Our data suggest that short-term increases in pHi in normal epithelial cells can drive transcriptional, protein, and activity changes in metabolic enzymes including key glycolytic regulators (such as lactate dehydrogenase) as well as enzymes like pyruvate dehydrogenase kinase which negatively regulates pyruvate dehydrogenase and integrates metabolite flux through various metabolic pathways. Thus, our results suggest that pHi may be a driving mechanism for metabolic reprogramming and not an outcome of metabolic reprogramming itself.

One of the well-established hallmarks of cancer is the metabolic reprograming of cells (Hanahan and Weinberg, 2011) as they switch from cellular respiration to a glycolytic metabolism. This process is also known as the Warburg effect (Liberti and Locasale, 2016). Our data show that just 24 hours of increased pHi can drive Warburg-like changes in metabolism, suggesting pHi may be initiating or reinforcing metabolic changes in tumorigenesis. Our transcriptional results show normal mammary epithelial cells upregulate glycolytic enzymes at high pHi and downregulate glycolytic enzymes at low pHi. Additionally, our biochemical data suggests that pHi may differentially regulate pyruvate fate to drive a glycolytic (Warburg-like) metabolism at increased pHi driven by increased expression of LDHA and PDK1 to drive conversion of pyruvate to lactate over AcCoA. Conversely, at the low pHi frequently seen in stem cells with bivalent metabolism (Zhou *et al.*, 2012), pH-dependent loss of LDHA and PDK1 may support preferential conversion of pyruvate to AcCoA. However, care must be taken not to over-interpret metabolic pathway changes as metabolic enzymes are allosterically regulated and metabolic flux is not always correlated to enzyme expression level. Moreover, prior computational approaches have suggested that increased pHi may promote changes in metabolic enzyme activity (Persi *et al.*, 2018). Persi *et al*. presented a computational prediction of changes in enzymatic activity based on pHi. Comparing Persi's results to our expression data, we found that a subset of genes such as CA9, G6PI, and PGK1 seem to be similarly regulated at the transcriptional level and enzymatic activity of the protein (Supplemental Table 5). Taken together, these data suggest that pHi may play multiple roles in the regulation of enzymatic activity and during the metabolic reprogramming. Future work will collect metabolomic data to

support these pHi-dependent transcriptional profiles and integrate the -omics datasets with published computational predicted activity mapping (Persi *et al.*, 2018).

Our data also suggests a role for increased pHi in driving increased Notch1 signaling in a normal genetic background. Notch1 signaling has been linked to pH-dependent processes like stem cell differentiation, cell cycle progression, and migration (Wang *et al.*, 2006; Matsumoto *et al.*, 2011; Shao *et al.*, 2015). However, the role for pHi in regulating Notch signaling has not been explored. Here, we showed that increased pHi drives increased Notch1 expression and downstream activation. This suggests that the transient increases in pHi (24 hours) observed during differentiation might drive or reinforce increased Notch activity important for temporal regulation of differentiation (Clevers, 2013; Ulmschneider *et al.*, 2016; Bohin *et al.*, 2020). Furthermore, these results open the possibility to use pHi to regulate Notch signaling and probe the impact of Notch signaling regulation in different biological contexts and processes.

In addition to its role in the normal cell behaviors described above, Notch1 upregulation has been shown to be tumorigenic (Yuan *et al.*, 2015) and associated with increased epithelial to mesenchymal transition (Shao *et al.*, 2015). Interestingly, Notch1 has been described to have oncogenic and tumor suppressor roles in the development of cancer and is implicated in the development of cardiovascular disease, but there has not yet been a link between these roles and pHi. We hope that our work will open new lines of research using pHi regulation of Notch1 as a target to prevent or treat Notch-related diseases.

Other interesting pH-sensitive gene transcription nodes identified include carbonic anhydrase 9 (CA9), Cyclin D1 (CCND1), and the F-box and WD repeat domain containing 7 (FBXW7) (Figure 2A, B; Supplemental Table 2). CA9 serves to generate extracellular bicarbonate and is upregulated at high pHi and downregulated at low pHi. Upregulation of CA9 is associated with increased proliferation and migration behaviors that are associated with increased pHi (Chiche *et al.*, 2009; Benej *et al.*, 2020). CA9 silencing, on the other hand, suppresses proliferation, promotes mitochondrial biogenesis, and reduces cell migration all behaviors associated with decreased pHi (Cianchi *et al.*, 2010; Csaderova *et al.*, 2013; Xu *et al.*, 2020). Our RNASeq data suggests that pHi-dependent regulation of CA9 expression may reinforce these pH-dependent processes.

Cyclin D1 (CCND1) is a crucial regulator of cell cycle progression with a distinct role in the transition from G1 to S. Overexpression of CCND1 has been linked to cancer progression by promoting inhibition of the retinoblastoma gene (Kato *et al.*, 1993) and it has also been shown to promote endocrine resistance to estrogen in breast cancer (Hui *et al.*, 2002). Additionally, CCND1 has been previously shown to be upregulated at high pHi leading to proliferation and tumor growth in retinal epithelial cells (Koch *et al.*, 2020). However, in this study we show that CCND1 is downregulated in human mammary epithelial cells at high pHi and upregulated at low pHi (Figure 2A, B; Supplemental Table 2). These findings are supported by prior data showing low pHi upregulates expression of CCND1 in mouse fibroblasts (Putney and Barber, 2004). This result dovetails with our recent work showing pHi is dynamic during the cell cycle and drives key transitions including exit from G1 and G2 entry (Spear and White, 2022). Thus the transcriptional results presented herein will guide future work characterizing the molecular drivers of pH-sensitive cell cycle progression.

Our work suggests that transient changes in pHi can promote global transcriptional changes in normal epithelial cells. This dataset provides a starting point to explore pHi-associated biomarkers, pH-sensitive pathway nodes, and pH-dependent transcriptional regulation in cell biology. Data presented here suggests that pHi changes are sufficient drivers of metabolic and

signaling changes associated with pH-dependent cell behaviors. Furthermore, our work suggests increased pHi is a sufficient driver of metabolic reprogramming in epithelial cells and supports further study of pHi changes as an early marker of metabolic reprogramming during normal cell processes like differentiation and EMT as well as the potential for high pHi to drive tumorigenic phenotypes in cancer.

Acknowledgments: We would like to thank Dr. Joe Sarro, Jacqueline Lopez, and Dr. Michael Pfrender form the Genomics & Bioinformatics Core at the University of Notre Dame for their help in the planning, execution, and analysis of the RNASeq experiments presented in this work. Notch activity reporter plasmid (CBF:H2B-Venus) was a gift from Anna-Katerina Hadjantonakis (Addgene plasmid #44211). This work was supported by an American Cancer Society-Institutional Research Grant (IRG), startup funds from the University of Notre Dame, and the Henry Luce Foundation. Figures 1A, 1E, 3A, 4A, 4B, and 4E were generated using BioRender software.

Author Contributions: K.A.W. and R.R.M. conceived the project and planned the experimental strategy. K.A.W. and R.R.M worked in collaboration with the Genomics & Bioinformatics Core at Notre Dame to design the RNASeq strategy. R.R.M. and J.F.K performed the experiments. R.R.M, J.F.K, and K.A.W. analyzed the data. R.R.M. and J.F.K created the figures. R.R.M. and K.A.W. wrote the manuscript. All authors edited and approved final submission of manuscript.

Declaration of interests: The authors declare no competing interests.

Supplemental Figures and Legends

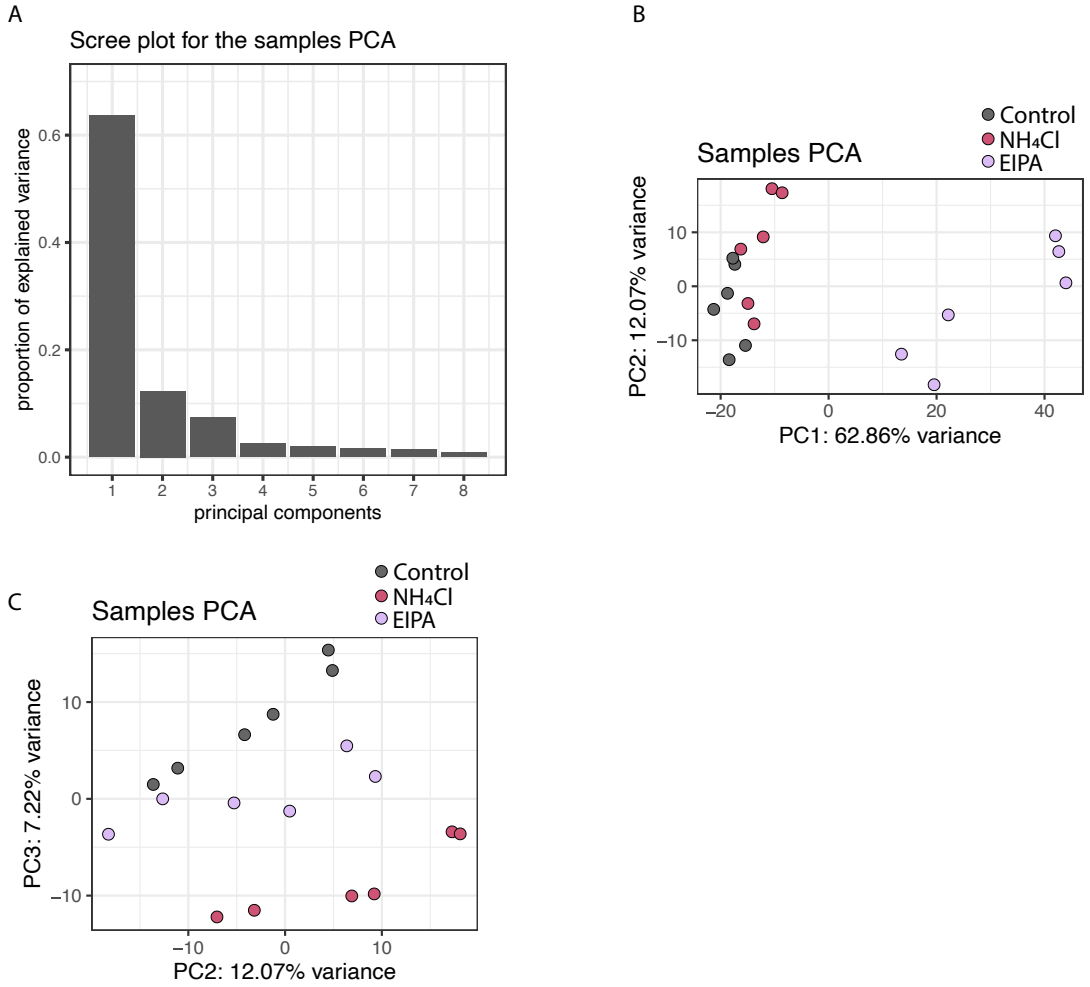

Figure S1. PCA of RNASeq shows that low (EIPA), normal (Control), and high (NH_4Cl) pHi MCF10A cells. A) Variance distribution of all principal components calculated in the Principal Component Analysis (PCA) of all 6 RNASeq biological replicates across the 3 different pHi treatment conditions (see methods). Component 1 accounts for just under 63% of the variance, component 2 describes about 12% of the variance, and component 3 describes just over 7% of the total variance in the dataset. B) PCA plot of components 1 and 2 shows a clear separation of low pHi samples from the normal and high pHi conditions. C) PCA plot of components 2 and 3 shows separation between the high pHi samples from the other two conditions.

Figure S2. All differentially regulated genes in the RNASeq dataset. Heatmap showing the significantly upregulated (magenta) and downregulated (cyan) genes found in the RNASeq data when compared to the control. Higher opacity corresponds to further deviation from the control sample.

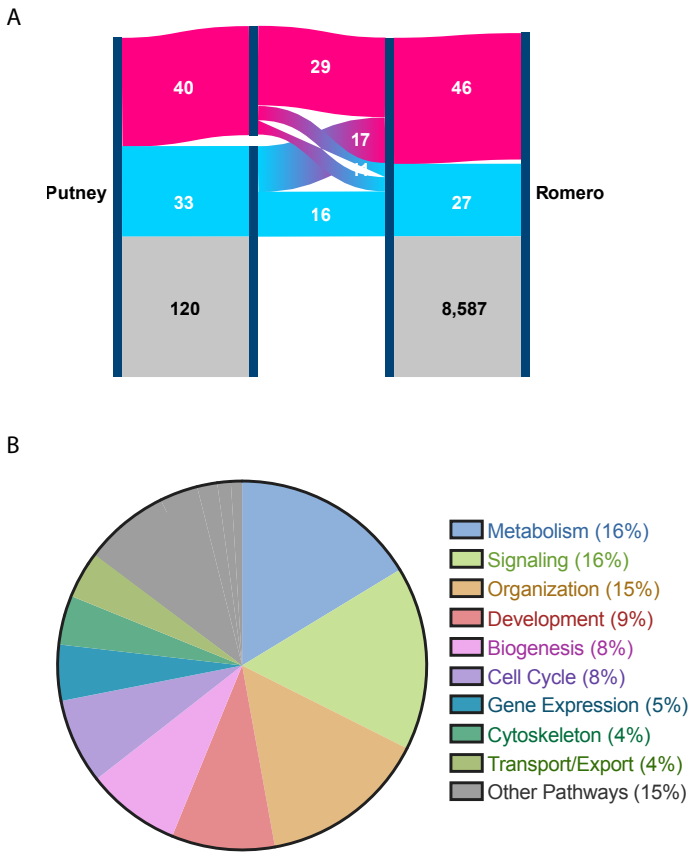

Figure S3. Comparison of gene expression profiles between low pHi (EIPA) and control cells. A) Sankey diagram showing the comparison of the low pHi vs. control mouse fibroblast microarray analysis from Putney et al (Putney and Barber, 2004) and our RNASeq analysis of low pHi vs. control normal human mammary epithelial cells. 45 genes showed similar transcriptional regulation between the datasets and 28 genes showed opposite regulatory effects across the two datasets. Upregulated genes are shown in magenta and downregulated genes are shown in cyan. B) Analysis of the top 500 Gene Ontology (GO) terms found in our RNASeq dataset. (Metacore GO analysis; see methods). All GO terms with 3% or lower representation were grouped as Other Pathways.

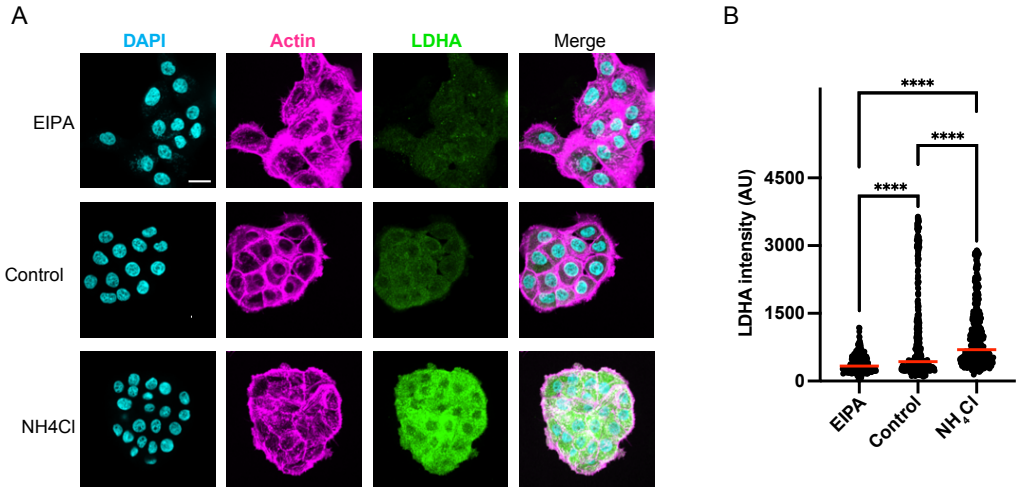

Figure S4. Immunofluorescent staining showing pH-dependent lactate dehydrogenase (LDHA) expression. MCF10A cells were incubated for 24 hours in 25 μM EIPA, normal media, or 30 mM NH_4Cl prior to imaging. Cells were then fixed and stained with their corresponding primary and secondary antibodies (see methods). A) Representative confocal images of MCF10A cells at low pHi (EIPA), control, and high pHi (NH_4Cl). LDHA fluorescence is shown in green, Phalloidin staining shown in magenta (Actin), and nuclei stain in cyan (DAPI). Scale bars: 20 μm. B) Quantification of LDHA fluorescent intensity from images collected as in A. Fluorescence intensity from individual cells are shown in scatter plot (mean±SEM) from 5 biological replicates. For B, significance determined using Kruskal-Wallis with Dunn's multiple comparisons correction; ****$p<0.0001$.

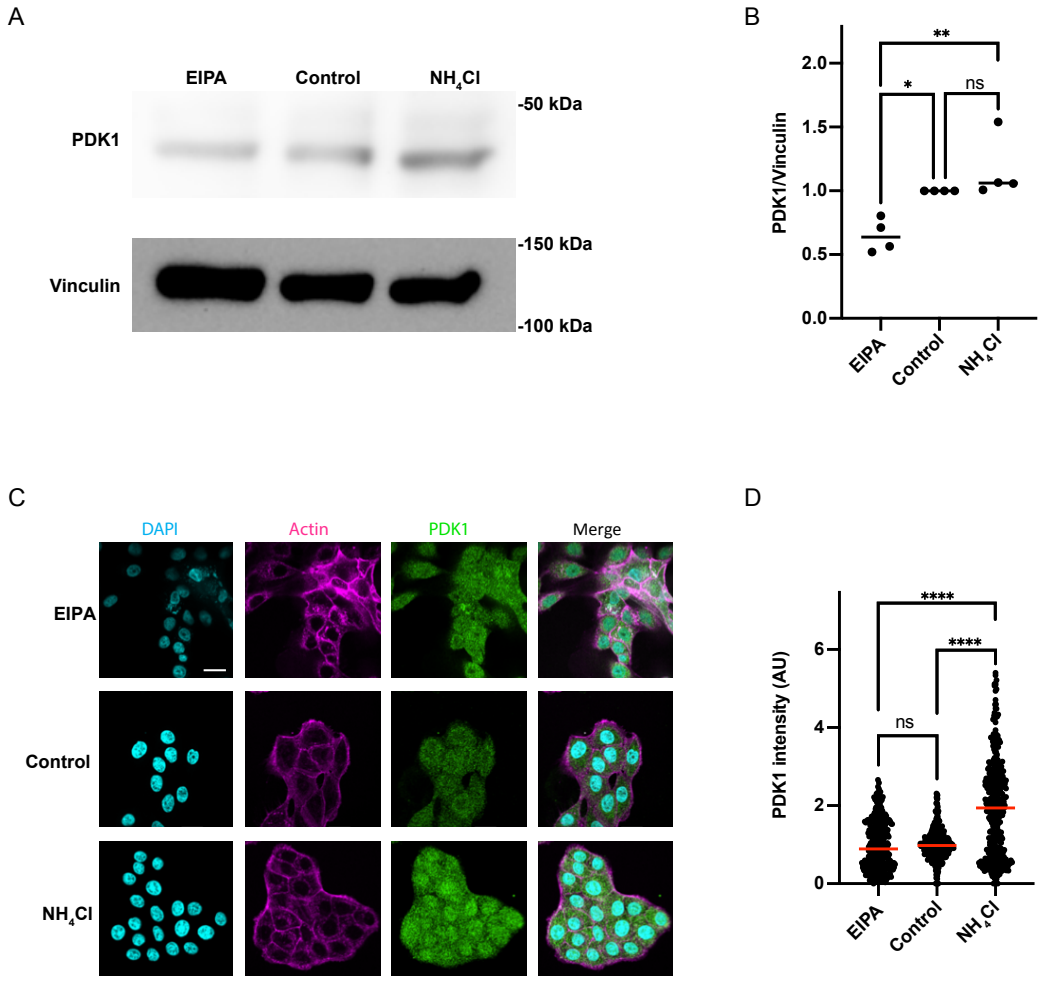

Figure S5. Immunofluorescent staining showing pH-dependent pyruvate dehydrogenase kinase (PDK1) expression. MCF10A cells were incubated for 24 hours in 25 μM EIPA, normal media, or 30 mM NH_4Cl prior to imaging. Cells were either lysed for protein isolation or fixed and stained with corresponding primary and secondary antibodies (see methods). A) Representative immunoblot for PDK1 and loading control (vinculin) from lysates of MCF10A cells at low pHi (EIPA), control, and high pHi (NH_4Cl). B) Quantification of immunoblots prepared as in A. PDK1 expression was normalized to vinculin loading control. Scatter plot (mean±SEM) from 4 biological replicates. C) Representative confocal images of MCF10A cells at low pHi (EIPA), control, and high pHi (NH_4Cl). PDK1 fluorescence is shown in green, Phalloidin staining shown in magenta (Actin), and nuclei stain in cyan (DAPI). Scale bars: 20 μm. D) Quantification of PDK1 fluorescent intensity from images collected as in C. Fluorescence intensity from individual cells are shown in scatter plot (mean±SEM) from 3 biological replicates. For B, significance determined using ANOVA with Tukey's multiple comparisons correction. For D, significance determined using Kruskal-Wallis with Dunn's multiple comparisons correction; *$p<0.05$, **$p<0.01$, ****$p<0.0001$.

Supplemental Table 1. Complete RNASeq Dataset. All transcripts sequenced and mapped to the human genome in the RNASeq dataset. First tab is all transcripts from low pHi (EIPA) compared to control MCF10A. Second tab is all transcripts from of high pHi (NH_4Cl) compared to control. Default sorting is by lowest False Discovery Rate (FDR).

Supplemental Table 2. All significantly altered transcripts in the RNASeq dataset. First tab is all transcripts significantly altered at low pHi (EIPA) compared to control MCF10A. Second tab is all transcripts significantly altered at high pHi (NH_4Cl) compared to control. Default sorting is alphabetical.

Supplemental Table 3. All differentially regulated transcripts in the RNASeq dataset. First tab is all transcripts significantly upregulated at low pHi (EIPA) and downregulated at high pHi (NH_4Cl) compared to control MCF10A. Second tab is all transcripts significantly downregulated at low pHi (EIPA) and upregulated at high pHi (NH_4Cl) compared to control MCF10A. Default sorting is alphabetical.

Supplemental Table 4. Comparison between Putney *et al.* mouse microarray dataset and Romero *et al.* human RNASeq dataset. First tab is the list of all transcripts found in common between the two datasets and organized as described in Putney *et al.* (Putney and Barber, 2004). Second tab is all transcripts in common listed in alphabetical order. Third tab is only transcripts with matched regulation between the two datasets (concordant data). Fourth tab is only transcripts with opposite regulation between the two datasets (non-concordant data).

Supplemental Table 5. Comparison between Persi *et al.* computational enzymatic activity prediction and Romero *et al.* human RNASeq dataset. First tab is transcripts found in common between our RNASeq data set and the predicted behavior of the metabolic enzymes described in Persi *et al.* (Persi *et al.*, 2018). Second tab is only transcripts with matched directionality between the two datasets (concordant data). Third tab is only transcripts with mismatched directionality between the two datasets (non-concordant data).

Materials and Methods:

Cell culture

Cells were maintained in humidified incubators at 37°C with 5% CO_2. MCF10A cells (ATCC: CRL-10317) were split at sub-confluency and discarded when passaged 30 times after thawing. Cells were monitored for maintenance of epithelial morphology throughout experimental protocols.

MCF10A complete media: DMEM/50% F12 w/ GlutaMax (Invitrogen, 10565-018) supplemented with 5% Horse Serum (Invitrogen, 16050-122), 0.02 ug/mL EGF (Peprotech, AF-100-15), 5 ug/mL Hydrocortisone (Sigma, H-0888), 10 mg/mL Insulin (Sigma, I-1882), 0.1 ug/mL Cholera toxin (Sigma, C-8052), and 1% Penicillin- Streptomycin (Corning, 30-001-CI).

pHi manipulation media:
Control: Complete media
Low pHi: Complete media supplemented with 25 µM EIPA (Invitrogen, E3111)
High pHi: Complete media supplemented with 30 mM ammonium chloride (NH_4Cl, Fisher Chemical, A661-500, Lot 185503)

All chemical concentrations are final concentrations (C_f).

pHi measurement and calculation

MCF10A cells were plated in triplicate for each treatment condition ($3x10^4$ cells/well; 24 well plate; 1 mL total volume). 24 hours after plating, media was removed and pHi manipulation media (see above) was added to the cells. After 24 hours of incubation with pHi manipulation media, pHi was measured as previously described (Choi *et al.*, 2013; White *et al.*, 2017). Briefly, 2',7'-Bis-(2-Carboxyethyl)-5-(and-6)- Carboxyfluorescein, Acetoxymethyl (BCECF-AM) Ester (Biotium, 51011) was added at 2 µM (C_f) to cells for 30 min at 37°C with 5% CO_2. Cells were then washed 3X 5 min with HEPES-based wash buffer (30 mM HEPES, 145 mM NaCl, 5 mM KCl, 10 mM glucose, 1 mM KPO_4, 1 mM $MgSO_4$, and 2 mM $CaCl_2$) at 37°C with 5% CO_2. Wash buffers were supplemented with appropriate pH-altering compounds at the same concentrations as the 24 hr incubations. After washes, fluorescence was read on a plate reader (Molecular Devices Spectramax M3) at the pH-sensitive wavelengths (490ex/535em) and the pH-insensitive wavelengths (440ex/535em) was acquired every 15sec for 5 minutes at Medium PMT sensitivity. After the initial pHi read, wash buffers were removed and replaced with a ~7.6 pH nigericin buffer standard (25 mM HEPES, 80 mM KCl, 1 mM $MgCl_2$) supplemented with 10 µM nigericin (Invitrogen, N1495). Cells were incubated at 37°C for 10 min, and the plate was read again with the same parameters. The high nigericin buffer was then replaced with a ~6.6 pH nigericin buffer standard, cells were incubated at 37°C for 10 min, and the plate was read again with the same parameters. Mean intensities from pHi measurement and the nigericin standards were exported and pHi was back-calculated using a nigericin linear regression performed on each individual well.

Trypan blue exclusion assay

Cells were plated at 30,000 cells per well in a 24 well plate. 24 hours after plating, cells were incubated for 24 hours in 30 mM NH_4Cl, 25 µM EIPA, or fresh media in a 24-well plate. After the 24 h incubation period, the media supernatant was removed and we washed the cells with 2 ml of prewarmed 1xDPBS (Lonza, 17-512F). The PBS was then removed and cells were then incubated at 37°C in 250 µL of trypsin (Corning, 25-053-CI) for about 13-15 minutes until cells started to come off the plate. After incubation in trypsin, 250 µL of prewarmed full culture media was added to each well to inactivate the trypsin. Cells were gently resuspended with care to

avoid clumps, then 50 μL of the resuspended cells were added to an Eppendorf tube. Just before counting, 50 μL of trypan blue 0.4% solution (Gibco, 15250-061) was added to the Eppendorf tube and mixed well. 10 μL of the trypan blue and suspended cells mixture was counted on a hemocytometer for healthy (clear) cells and unhealthy/dying (blue) cells. Each biological replicate is the average of three technical replicates (three different wells for each condition). Each biological replicate was assessed from cells plated on a different day. Counts of the multiple conditions were performed in batches to avoid long exposure to trypsin, formation of clumps, or over-incubation in trypan blue.

RNA extraction and sequencing

From a single parental 10 cm plate of MCF10A cells, when the plate reached a confluency of ~85%, cells were split 1:6 into three plates. 24 hours later, each one of these three plates was split into two plates that would serve as two technical replicates for each experimental condition (control, 30 mM NH_4Cl, 25 μM EIPA). After 48 hours following the second passage, media was changed with the appropriate concentration of the pH-altering compounds and incubated at 37°C with 5% CO_2 for 24 hours. After the 24-hour incubation in pHi-altering treatment, plates were quickly washed 2X with ice cold PBS and then total RNA was extracted following manufacturer's protocol (RNeasy Plus Minikit (Qiagen, 74134) and RNA concentration and purity was assessed (Thermo Fisher, NanoDrop One).

Sequencing Strategy was developed in collaboration with the Notre Dame Genomics Core: Eighteen (18) total RNASeq libraries were prepared (three different conditions and six replicates per condition) and sequenced across two lanes of an Illumina NextSeq v2.5 (75 cycle) flow cell. Each library was prepared using the NEBNext Poly(A) mRNA Magnetic Isolation Module and NEBNext Ultra II Directional RNA Library Prep kit. QC and quantitation on the library pool were performed using the Qubit dsDNA, Agilent Bioanalyzer DNA 7500 Chip, and Kapa Illumina Library Quantification qPCR assays. Sequencing format was single-read 75bp. Base calling was done by Illumina Real Time Analysis (RTA) v2 software.

Raw sequences were trimmed of adapters with Trimmomatic version 0.39 (Bolger, Lohse and Usadel, 2014) and assessed for quality with FastQC v 0.11.8 (Babraham Bioinformatics). Trimmed sequences were aligned to the human genome, Ensembl build Homo_sapiens.GRCh38, using Homo_sapiens.GRCh38.101 version annotations (Zerbino *et al.*, 2018) and HISAT2 version 2.1.0 (Kim *et al.*, 2019). Corresponding alignments were sorted with SAMtools version 1.9 (Li *et al.*, 2009). Read counts were generated with HTSeq-count version 0.11.2 (Anders, Pyl and Huber, 2015) and were merged with a python script. Subsequent statistics were completed in R (R Core Team, 2014) implementing the EdgeR library (Robinson and Smyth, 2007, 2008; Robinson, McCarthy and Smyth, 2009; McCarthy, Chen and Smyth, 2012). Gene names and GO terms were identified using the Ensembl version of BioMart (Kinsella *et al.*, 2011).

For pathway analysis and determination of target for biochemical validation, a False Discovery Rate (FDR) < 0.05 cutoff was applied to our RNASeq analysis. Log_2 fold change (log_2FC) < -0.5 values were considered downregulated and $log_2FC > 0.5$ values were considered upregulated for each one of our conditions when compared to the control.

MetaCore Pathway Analysis

After processing the RNASeq data, a table was uploaded to MetaCore containing the mapped gene ID, the log_2 Fold Change, and the False Discovery Rate for each of the comparisons (EIPA v. control, and NH_4Cl v. Control). MetaCore is a manually curated software that builds

ontologies mapped to canonical pathways and networks. Once the data was successfully uploaded to MetaCore, the canonical pathway maps analysis was run. This type of analysis results in a list of the pathway maps with the highest z-score for all of the maps in each of our different experimental conditions. The z-score is calculated as follows z-score = (Actual - Expected) * N * sqrt(N-1) / sqrt(n*R*(N-n)*(N-R)) where Actual is the number of affected genes in a dataset, expected is the mean value for the hypergeometric distribution (n*R/N), N is the total number of node on the MetaCore database, n is the total number of nodes in each small network generated from our list, R is the number of the network's objects corresponding to the genes in our list. And the variance is calculated as follows variance = n*R*(N-n)*(N-R) / (N*N*(N-1)).

Western Blots

From a single parental 10 cm plate of MCF10A cells, cells were split 1:6 into three plates. 24 hours later, media was changed with the appropriate concentration of the pH-altering compounds (control, 30 mM NH_4Cl, 25 µM EIPA) and incubated at 37°C with 5% CO_2 for 24 hours. After the 24-hour incubation in pHi-altering treatment, plates were quickly washed 2X with ice cold PBS and then 500 µL of ice-cold lysis buffer (50mM Tris, 150 mM NaCl, 1 mM EDTA, 1 mM DTT, 1 mM Na_3VO_4, 1 mM NaF, 1% TritonX-100, and a protease inhibitor cocktail (Pierce™ Protease Inhibitor Tablets, A32965; 1 tablet/50 mL of lysis buffer), pH 7.4) and plates were incubated on ice for 15 minutes. Cell were then scraped off the plate and transferred into a 1.5 mL Eppendorf tube and pipetted up and down a couple of times to ensure proper lysis of the cell membrane. Cell lysates were then spun down at max speed in a countertop centrifuge at 4 ^{o}C for 10 minutes. The clear supernatant was then carefully transferred to a new tube and stored at -80 ^{o}C until further analysis. Protein concentration was assessed by BCA assay (Thermo Scientific, 34580) using the standard manufacturer protocol.

20 µg of protein lysate was mixed with Laemmli loading buffer (Alfa Aestar, J61337-AC), boiled for five minutes, loaded onto gels (10% Bio-Rad Mini-PROTEAN® TGX Stain-Free™ Precast Gels, 10026447), and electrophoresed in running buffer (25 mM Tris, 192 mM Glycine, 0.1% SDS) at 100V for 2 hours. Proteins were transferred to a PVDF membrane (Millipore Immobilion-P, IPVH00010) using a wet transfer with freshly made transfer buffer (25 mM Tris, 192 mM Glycine, 20% Methanol) at 60V for 1.5 hours. Prior to transfer, PVDF membranes were soaked for 5 minutes in 100 methanol and then washed 3X with ddH_2O. After transferring, membranes were blocked with 5% dry milk (or 5% BSA for phospho-antibodies) in 1x TBST (20 mM Tris, 137 mM NaCl, 0.1% Tween, pH 7.6 with HCl) for one hour and then divided for blotting on the basis of the prestained protein ladder (Bio-Rad, 1610373). Primary antibodies (see antibody table for vendor and dilutions) diluted in 5% BSA were incubated overnight at 4°C in followed by 3 x 5-minute washes with 1xTBST and a 1-hour incubation with an HRP-conjugated secondary antibody followed by another 3 x 5-minute wash with 1xTBST. Chemiluminescence was induced by incubating the membranes for 3-5 minutes in the SuperSignal™ West Pico PLUS Chemiluminescent Substrate (Thermo Scientific, 34580). Images were captured through a gel imager (Bio-Rad, ChemiDoc MP).

Western blot analysis was performed using ImageJ densitometry analysis. Each band was enclosed using a rectangular selection of the same size, a densitometry histogram was plotted for the selected experimental and loading control bands. Background was subtracted using the straight-line tool and area under the enclosed curve was acquired. The ratio of the protein of interest normalized to loading control was calculated from exported densitometry data.

Target	Host	Dilution	Company	Cat #	Type	Experiment
NOTCH1	Rabbit	1:1000, 1:400	Cell Signaling	3608S	Primary	WB, ICC
LDHA	Rabbit	1:1000	Cell Signaling	3582S	Primary	WB
β-Tubulin	Rabbit	1:1000	Abcam	ab6046	Primary	Loading control
Vinculin	Rabbit	1:1000	Cell Signaling	13901S	Primary	Loading control
Anti-rabbit AlexaFluor 488	Goat	1:1000	Invitrogen	A11008	Secondary	ICC
Phalloidin-AlexaFluor 647	N/A	1:1000	Invitrogen	A22287	Actin Stain	ICC
Anti-mouse HRP	Goat	1:1000	Southern Biotech	1030-05	Secondary	WB
Anti-rabbit HRP	Goat	1:1000	Southern Biotech	1050-05	Secondary	WB

Microscopy

All imaging experiments were performed using a Nikon Ti2 Eclipse confocal microscope equipped with a spinning disk (CSU-X1, Yokogawa) using solid-state lasers (395 nm, 488 nm, 561 nm) with appropriate filter sets (DAPI: ET455/50M, mVENUS: ET525/36M, AF561: ET561/60M) on 40x objective (CFI Plan Fluor 40X, NA =1.30, MRH01401, NIKON), using a CMOS camera (ORCA-Flash4.0). Cells were imaged in 35 mm imaging dishes (Matsunami, Dd35-14-1.5-U) within a stage-top environmental chamber (Tokai) at 37°C and 5% CO_2. All microscope control and image analyses used Nikon NIS Elements AR software.

Notch activity assay

Notch activity reporter (CBF:H2B-Venus) was a gift from Anna-Katerina Hadjantonakis (Addgene plasmid #44211) (Nowotschin *et al.*, 2013). MCF10A cells were grown in a 10 cm dish until they reached 70-80% confluency and then were transfected with CBF:H2B-Venus using manufacturer's protocol (FuGene HD, Promega, E2311). Briefly, 450 μL of room temperature serum-free media were added to a 0.6 mL Eppendorf tube, 10 μg of DNA was then

added to the Eppendorf tube and mixed by inverting the tube 4-5 times. Then, 30 μL of the transfection reagent (Fugene HD) was added to the tube (3:1 Fugene HD to DNA ratio, μL:μg), mixed again by inverting the tube 4-5 times and then let incubate at room temperature for 15 minutes. After the 15-minute incubation, the contents of the Eppendorf tube were combined with 4.5 mL of pre-warmed full media and then the mixture was added to the 10 cm plate of cells and incubated at 37 ^{o}C. Cells were incubated with transfection media for 6 hours and then trypsinized (0.25% Trypsin EDTA, Corning, 25-053-CI), plated in triplicate (25,000 cells/dish; 35 mm imaging dishes: Matsunami, Dd35-14-1.5-U), and then returned to the incubator overnight. 24 hours post-transfection, dishes were treated with pHi manipulation media (control, 25 μM EIPA, and 30 mM NH_4Cl). 48 hours post-transfection (24 hours post pHi manipulation) dishes were imaged by confocal microscopy. A minimum of 10 fields of view were taken using a GFP laser (488 nm excitation, 400 ms, 25% power), a DAPI laser (405 nm excitation, 300 ms, 15% power), and a DIC image (300 ms) using a 40x oil immersion objective. Images were processed and analyzed using Nikon Elements AR software. Images were background subtracted using an ROI placed on an area without cells within each field of view. ROIs were drawn on each cell using the mVenus fluorescence signal, and average ROI intensity values were obtained for each cell's mVenus signal. To account for artifactual fluorescence caused, a separate 10 cm plate of cells was mock transfected (same protocol as above without DNA) and imaging was conducted as described above for all of our conditions. Two times the average fluorescence in these mock transfected cells was used as a cutoff for inclusion in the analysis.

LDH assay

The lactate dehydrogenase colorimetric assay (Abs_{450}) kit (Sigma, MAK066) measures LDH activity in a biological sample based on reduction of NAD to NADH. The amount of NADH generated is used to back-calculate the milliunits/mL of LDH in the biological sample using a linear regression of known standards. For each condition, $1x10^6$ cells were lysed in 500 μL of the assay buffer provided in the kit and 2 μL of the lysed cells were used for analysis. For the rest of the analysis, the manufacturer's standard protocol was followed. Assays were run in technical duplicates and averaged for each data point.

Lactate assay

The lactate assay kit (Sigma, MAK066) is a colorimetric assay that measures lactate concentration (0.2–10 nmoles of lactate) in a biological sample and is determined by an enzymatic assay leading to a readout that is proportional to the lactate present in the sample. The lactate concentration in the biological sample can be back-calculated from the read measurement (Abs_{570})/fluorometric (λ_{ex535}/ λ_{em587}) using a linear regression of known standards. For each condition, $1x10^6$ cells were lysed in 500 μL of the assay buffer provided in the kit. After lysing the cells, samples were spun at 10,000 x g for 10 minutes in a 10 kDa size exclusion tube (EMD Millipore, UFC801024) to remove proteins, with the flow-through retained for further analysis. 2 μL of the extracted cell lysate was used for analysis. For the rest of the analysis, the manufacturer's standard protocol was used. Assays were run in technical duplicates and averaged for each data point.

Immunofluorescence Assays

Cells were trypsinized and 80,000 MCF10A cells were plated in each of three 3.5 cm imaging dishes (Matsunami, Dd35-14-1.5-U) and returned to the incubator for 24 hours. Cells were then treated with pHi-manipulation media and dishes were returned to the incubator overnight. 24 hours after treatment, cells were rinsed with PBS and fixed in 3.7% formaldehyde (Alfa Aestar, 33314) in DPBS at room temperature for 10 minutes. Cells were washed 3x2 min with DPBS, then incubated in antibody buffer (0.1% Triton-X, 1.0% BSA in DPBS) for 10 minutes at room

temperature. Cells were washed 3 x 2 min with DPBS, then incubated in blocking buffer (1.0% BSA in DPBS) for 1 hour at RT with rocking followed by 3 x 2 min wash in DPBS. Cells were then incubated overnight at 4°C in primary antibodies (see antibody table for vendor/cat and dilutions) in antibody buffer. After incubation with primary antibody, cells were washed 3 x 2 min in DPBS, then incubated with secondary antibodies (see antibody table for vendor/cat and dilutions), Phalloidin conjugate, and 1:20,000 dilution of Hoescht dye in antibody buffer for one hour at room temperature in the dark with gentle rocking. After a final 3 x 2 min wash in PBS, cells were imaged using a Nikon Ti2 Eclipse confocal microscope equipped with a spinning disk microscope (CSU-X1, Yokogawa). A minimum of 5 fields of view per dish were acquired using the following settings: (AF488: 10% laser power, 500 ms; AF647: 10% laser power, 500 ms; DAPI: 10% laser power, 150 ms), and a DIC image (50 ms). The acquired images were then analyzed using the Nikon NIS Elements AR software as follows: A rectangular ROI on the glass coverslip was used to subtract the background from the current frame in each field of view. Bezier ROIs were used to select each cell as a region of interest. ROIs were saved, and data with GFP intensity values for each ROI was exported into Excel. These data were imported into GraphPad Prism for analysis. After collecting all biological replicates, the ROUT (Q=1%) method was used to identify and remove outliers and Shapiro-Wilk normality tests run in PRISM 9. For non-normally distributed data, a Kruskal-Wallis test with Dunn's multiple comparisons test was used to identify significant differences between the EIPA, control, and NH_4Cl. The mean rank of each column was compared with the mean rank of every other column.

Statistical analyses summary

For all data consisting of 10 data points or more, a Shapiro-Wilk normality test was used to determine normality of the data distribution. For normally distributed data or data samples smaller than 10 data points, statistical significance was determined using a one-way ANOVA with Tukey multiple-comparisons correction. For non-normally distributed data, statistical significance was determined using Kruskal−Wallis test with Dunn's multiple-comparisons correction.

FIGURE PREAPRATION DETAILS/SOFTWARE
PCA/METACORE/SANKEY

Figures 1A, 1E, 3A, 4A, 4B, and 4E were prepared using BioRender.com
Figures 1B, 1C, 3C, 3D, 3E, 4D, 4G, S4B, S5B, and S5D were prepared using Prism 9
Figures 1D, 4F, S4A, and S5C were prepared using the Nikon NIS Elements AR software
Figures 2A, 2B, S1A, S1B, S1C and S2 were created using R/RStudio or PCAExplorer package for R and modified in Adobe Illustrator
Figures 2C and S3A were created using sankeymatic.com and modified in Adobe Illustrator
Figure S3B was created using Microsoft Excel and modified in Adobe Illustrator
Metacore (Clarivate) was used to analyze RNASeq datasets. From these analyses, we generated simplified pathways including only genes contained in our dataset for Figure 3A and 4A.

References

Alfarouk, K. O. *et al.* (2020) 'The pentose phosphate pathway dynamics in cancer and its dependency on intracellular pH', *Metabolites*. doi: 10.3390/metabo10070285.

Amith, S. R., Wilkinson, J. M. and Fliegel, L. (2016) 'Na+/H+ exchanger NHE1 regulation modulates metastatic potential and epithelial-mesenchymal transition of triplenegative breast cancer cells', *Oncotarget*, 7(16). doi: 10.18632/oncotarget.8520.

Anders, S., Pyl, P. T. and Huber, W. (2015) 'HTSeq-A Python framework to work with high-throughput sequencing data', *Bioinformatics*. doi: 10.1093/bioinformatics/btu638.

Andersen, A. P. *et al.* (2016) 'Roles of acid-extruding ion transporters in regulation of breast cancer cell growth in a 3-dimensional microenvironment', *Molecular Cancer*, 15(1). doi: 10.1186/s12943-016-0528-0.

Andersson, E. R., Sandberg, R. and Lendahl, U. (2011) 'Notch signaling: simplicity in design, versatility in function.', *Development (Cambridge, England)*. Oxford University Press for The Company of Biologists Limited, 138(17), pp. 3593–612. doi: 10.1242/dev.063610.

Benej, M. *et al.* (2020) 'CA IX Stabilizes Intracellular pH to Maintain Metabolic Reprogramming and Proliferation in Hypoxia', *Frontiers in Oncology*, 10. doi: 10.3389/fonc.2020.01462.

Bhattacharya, D., Azambuja, A. P. and Simoes-Costa, M. (2020) 'Metabolic Reprogramming Promotes Neural Crest Migration via Yap/Tead Signaling', *Developmental Cell*, 53(2). doi: 10.1016/j.devcel.2020.03.005.

Blanpain, C. *et al.* (2006) 'Canonical notch signaling functions as a commitment switch in the epidermal lineage', *Genes and Development*, 20(21). doi: 10.1101/gad.1477606.

Bohin, N. *et al.* (2020) 'Rapid Crypt Cell Remodeling Regenerates the Intestinal Stem Cell Niche after Notch Inhibition', *Stem Cell Reports*, 15(1). doi: 10.1016/j.stemcr.2020.05.010.

Bolger, A. M., Lohse, M. and Usadel, B. (2014) 'Trimmomatic: A flexible trimmer for Illumina sequence data', *Bioinformatics*. doi: 10.1093/bioinformatics/btu170.

Bouras, T. *et al.* (2008) 'Notch Signaling Regulates Mammary Stem Cell Function and Luminal Cell-Fate Commitment', *Cell Stem Cell*, 3(4). doi: 10.1016/j.stem.2008.08.001.

Chaumeil, M. M. *et al.* (2012) 'pH as a biomarker of neurodegeneration in Huntington's disease: a translational rodent-human MRS study.', *Journal of cerebral blood flow and metabolism : official journal of the International Society of Cerebral Blood Flow and Metabolism*. SAGE Publications, 32(5), pp. 771–9. doi: 10.1038/jcbfm.2012.15.

Chiche, J. *et al.* (2009) 'Hypoxia-inducible carbonic anhydrase IX and XII promote tumor cell growth by counteracting acidosis through the regulation of the intracellular pH', *Cancer Research*, 69(1). doi: 10.1158/0008-5472.CAN-08-2470.

Choi, C. H. *et al.* (2013) 'Ph sensing by FAK-His58 regulates focal adhesion remodeling', *Journal of Cell Biology*, 202(6). doi: 10.1083/jcb.201302131.

Cianchi, F. *et al.* (2010) 'Selective inhibition of carbonic anhydrase IX decreases cell proliferation and induces ceramide-mediated apoptosis in human cancer cells', *Journal of Pharmacology and Experimental Therapeutics*, 334(3). doi: 10.1124/jpet.110.167270.

Clevers, H. (2013) 'XThe intestinal crypt, a prototype stem cell compartment', *Cell*. doi: 10.1016/j.cell.2013.07.004.

Csaderova, L. *et al.* (2013) 'The effect of carbonic anhydrase IX on focal contacts during cell spreading and migration', *Frontiers in Physiology*, 4 OCT. doi: 10.3389/fphys.2013.00271.

Czowski, B. J. *et al.* (2020) 'Cancer and pH dynamics: Transcriptional regulation, proteostasis, and the need for new molecular tools', *Cancers*. doi: 10.3390/cancers12102760.

Damaghi, M., Wojtkowiak, J. W. and Gillies, R. J. (2013) 'pH sensing and regulation in cancer.', *Frontiers in physiology*. Frontiers Media SA, 4, p. 370. doi: 10.3389/fphys.2013.00370.

Denker, S. P. and Barber, D. L. (2002) ‘Cell migration requires both ion translocation and cytoskeletal anchoring by the Na-H exchanger NHE1.’, *The Journal of cell biology*. The Rockefeller University Press, 159(6), pp. 1087–96. doi: 10.1083/jcb.200208050.

Druzhkova, I. N. *et al.* (2016) ‘The metabolic interaction of cancer cells and fibroblasts – coupling between NAD(P)H and FAD, intracellular pH and hydrogen peroxide’, *Cell Cycle*, 15(9). doi: 10.1080/15384101.2016.1160974.

Fields, R. D. and Lancaster, M. V. (1993) ‘Dual-attribute continuous monitoring of cell proliferation/cytotoxicity.’, *American biotechnology laboratory*, 11(4).

Frantz, C. *et al.* (2007) ‘Positive feedback between Cdc42 activity and H+ efflux by the Na-H exchanger NHE1 for polarity of migrating cells’, *Journal of Cell Biology*, 179(3). doi: 10.1083/jcb.200704169.

Frantz, C. *et al.* (2008) ‘Cofilin is a pH sensor for actin free barbed end formation: role of phosphoinositide binding’, *Journal of Cell Biology*, 183(5). doi: 10.1083/jcb.200804161.

Gorbatenko, A. *et al.* (2014) ‘Regulation and roles of bicarbonate transporters in cancer’, *Frontiers in Physiology*, 5 APR. doi: 10.3389/fphys.2014.00130.

Hanahan, D. and Weinberg, R. a. (2011) ‘Hallmarks of cancer: The next generation’, *Cell*, 144(5), pp. 646–674. doi: 10.1016/j.cell.2011.02.013.

He, Y. and Zou, L. (2019) ‘Notch-1 inhibition reduces proliferation and promotes osteogenic differentiation of bone marrow mesenchymal stem cells’, *Experimental and Therapeutic Medicine*. doi: 10.3892/etm.2019.7765.

Hui, R. *et al.* (2002) ‘Constitutive overexpression of cyclin D1 but not cyclin E confers acute resistance to antiestrogens in T-47D breast cancer cells’, *Cancer Research*, 62(23).

Kang, H. *et al.* (2019) ‘Role of metabolic reprogramming in epithelial–mesenchymal transition (EMT)’, *International Journal of Molecular Sciences*. doi: 10.3390/ijms20082042.

Kato, J. *et al.* (1993) ‘Direct binding of cyclin D to the retinoblastoma gene product (pRb) and pRb phosphorylation by the cyclin D-dependent kinase CDK4’, *Genes and Development*, 7(3). doi: 10.1101/gad.7.3.331.

Kim, D. *et al.* (2019) ‘Graph-based genome alignment and genotyping with HISAT2 and HISAT-genotype’, *Nature Biotechnology*. doi: 10.1038/s41587-019-0201-4.

Kinsella, R. J. *et al.* (2011) ‘Ensembl BioMarts: A hub for data retrieval across taxonomic space’, *Database*. doi: 10.1093/database/bar030.

Koch, L. M. *et al.* (2020) ‘Cytosolic pH regulates proliferation and tumour growth by promoting expression of cyclin D1’, *Nature Metabolism*, 2(11). doi: 10.1038/s42255-020-00297-0.

Lagadic-Gossmann, D., Huc, L. and Lecureur, V. (2004) ‘Alterations of intracellular pH homeostasis in apoptosis: origins and roles’, *Cell Death & Differentiation*. Nature Publishing Group, 11(9), pp. 953–961. doi: 10.1038/sj.cdd.4401466.

Lázaro-Diéguez, F. *et al.* (2006) ‘Actin filaments are involved in the maintenance of Golgi cisternae morphology and intra-Golgi pH’, *Cell Motility and the Cytoskeleton*, 63(12). doi: 10.1002/cm.20161.

Li, H. *et al.* (2009) ‘The Sequence Alignment/Map format and SAMtools’, *Bioinformatics*. doi: 10.1093/bioinformatics/btp352.

Liberti, M. V. and Locasale, J. W. (2016) ‘The Warburg Effect: How Does it Benefit Cancer Cells?’, *Trends in Biochemical Sciences*. doi: 10.1016/j.tibs.2015.12.001.

Man, C. H. *et al.* (2022) ‘Proton export alkalinizes intracellular pH and reprograms carbon metabolism to drive normal and malignant cell growth’, *Blood*, 139(4). doi: 10.1182/blood.2021011563.

Matsumoto, A. *et al.* (2011) ‘Fbxw7-dependent degradation of notch is required for control of “Stemness” and neuronal-glial differentiation in neural stem cells’, *Journal of Biological*

Chemistry, 286(15). doi: 10.1074/jbc.M110.194936.

McCarthy, D. J., Chen, Y. and Smyth, G. K. (2012) 'Differential expression analysis of multifactor RNA-Seq experiments with respect to biological variation', *Nucleic Acids Research*. doi: 10.1093/nar/gks042.

Micchelli, C. A. and Perrimon, N. (2006) 'Evidence that stem cells reside in the adult Drosophila midgut epithelium', *Nature*, 439(7075). doi: 10.1038/nature04371.

Mosier, J. A. *et al.* (2021) 'Cancer cell metabolic plasticity in migration and metastasis', *Clinical and Experimental Metastasis*. doi: 10.1007/s10585-021-10102-1.

Mosmann, T. (1983) 'Rapid colorimetric assay for cellular growth and survival: Application to proliferation and cytotoxicity assays', *Journal of Immunological Methods*, 65(1–2). doi: 10.1016/0022-1759(83)90303-4.

Nomura, T. *et al.* (2022) 'Temperature sensitivity of Notch signaling underlies species-specific developmental plasticity and robustness in amniote brains', *Nature Communications*, 13(1). doi: 10.1038/s41467-021-27707-5.

Nowotschin, S. *et al.* (2013) 'A bright single-cell resolution live imaging reporter of Notch signaling in the mouse', *BMC Developmental Biology*, 13(1). doi: 10.1186/1471-213X-13-15.

Perez-Sala, D., Collado-Escobar, D. and Mollinedo, F. (1995) 'Intracellular alkalinization suppresses lovastatin-induced apoptosis in HL-60 cells through the inactivation of a pH-dependent endonuclease', *Journal of Biological Chemistry*, 270(11). doi: 10.1074/jbc.270.11.6235.

Persi, E. *et al.* (2018) 'Systems analysis of intracellular pH vulnerabilities for cancer therapy', *Nature Communications*. Nature Publishing Group, 9(1), p. 2997. doi: 10.1038/s41467-018-05261-x.

Putney, L. K. and Barber, D. L. (2003) 'Na-H exchange-dependent increase in intracellular pH times G2/M entry and transition.', *The Journal of biological chemistry*. American Society for Biochemistry and Molecular Biology, 278(45), pp. 44645–9. doi: 10.1074/jbc.M308099200.

Putney, L. K. and Barber, D. L. (2004) 'Expression profile of genes regulated by activity of the Na-H exchanger NHE1.', *BMC genomics*. BioMed Central, 5(1), p. 46. doi: 10.1186/1471-2164-5-46.

Putney, L. K., Denker, S. P. and Barber, D. L. (2002) 'The Changing Face of the Na+/H+ Exchanger , NHE1: Structure, Regulation, and Cellular Actions', *Annual Review of Pharmacology and Toxicology*, 42(1), pp. 527–552. doi: 10.1146/annurev.pharmtox.42.092001.143801.

R Core Team (2014) 'R Core Team (2014). R: A language and environment for statistical computing.', *R Foundation for Statistical Computing, Vienna, Austria. URL http://www.R-project.org/.*

Read, J. A. *et al.* (2001) 'Structural basis for altered activity of M- and H-isozyme forms of human lactate dehydrogenase', *Proteins: Structure, Function and Genetics*, 43(2). doi: 10.1002/1097-0134(20010501)43:2<175::aid-prot1029>3.0.co;2-%23.

Reshkin, S. J., Greco, M. R. and Cardone, R. A. (2014) 'Role of pHi, and proton transporters in oncogene-driven neoplastic transformation', *Philosophical Transactions of the Royal Society B: Biological Sciences*. doi: 10.1098/rstb.2013.0100.

Robinson, M. D., McCarthy, D. J. and Smyth, G. K. (2009) 'edgeR: A Bioconductor package for differential expression analysis of digital gene expression data', *Bioinformatics*. doi: 10.1093/bioinformatics/btp616.

Robinson, M. D. and Smyth, G. K. (2007) 'Moderated statistical tests for assessing differences in tag abundance', *Bioinformatics*. doi: 10.1093/bioinformatics/btm453.

Robinson, M. D. and Smyth, G. K. (2008) 'Small-sample estimation of negative binomial

dispersion, with applications to SAGE data', *Biostatistics*. doi: 10.1093/biostatistics/kxm030.

Ruffin, V. A. *et al.* (2014) 'Intracellular pH regulation by acid-base transporters in mammalian neurons.', *Frontiers in physiology*. Frontiers Media SA, 5, p. 43. doi: 10.3389/fphys.2014.00043.

De Saedeleer, C. J. *et al.* (2014) 'Glucose deprivation increases monocarboxylate transporter 1 (MCT1) expression and MCT1-dependent tumor cell migration', *Oncogene*, 33(31). doi: 10.1038/onc.2013.454.

Schönichen, A. *et al.* (2013) 'Considering protonation as a posttranslational modification regulating protein structure and function', *Annual Review of Biophysics*, 42(1). doi: 10.1146/annurev-biophys-050511-102349.

Shao, S. *et al.* (2015) 'Notch1 signaling regulates the epithelial-mesenchymal transition and invasion of breast cancer in a Slug-dependent manner', *Molecular Cancer*, 14(1). doi: 10.1186/s12943-015-0295-3.

Siekmann, A. F. and Lawson, N. D. (2007) 'Notch signalling and the regulation of angiogenesis.', *Cell adhesion & migration*, 1(2). doi: 10.4161/cam.1.2.4488.

Spear, J. S. and White, K. A. (2022) 'Single-cell intracellular pH dynamics regulate the cell cycle by timing G1 exit and the G2 transition', *bioRxiv*, p. 2021.06.04.447151. doi: 10.1101/2021.06.04.447151.

Srivastava, J. *et al.* (2008) 'Structural model and functional significance of pH-dependent talin-actin binding for focal adhesion remodeling', *Proceedings of the National Academy of Sciences of the United States of America*, 105(38). doi: 10.1073/pnas.0805163105.

Stoeckelhuber, M. *et al.* (1996) 'Structure/function studies on the pH-dependent actin-binding protein hisactophilin in Dictyostelium mutants', *Journal of Cell Science*, 109(7). doi: 10.1242/jcs.109.7.1825.

Stransky, L., Cotter, K. and Forgac, M. (2016) 'The function of v-atpases in cancer', *Physiological Reviews*, 96(3). doi: 10.1152/physrev.00035.2015.

Tsogtbaatar, E. *et al.* (2020) 'Energy Metabolism Regulates Stem Cell Pluripotency', *Frontiers in Cell and Developmental Biology*. doi: 10.3389/fcell.2020.00087.

Ulmschneider, B. *et al.* (2016) 'Increased intracellular pH is necessary for adult epithelial and embryonic stem cell differentiation', *The Journal of Cell Biology*, 215(3), pp. 345–355. doi: 10.1083/jcb.201606042.

Wang, X. De *et al.* (2006) 'Notch signaling is required for normal prostatic epithelial cell proliferation and differentiation', *Developmental Biology*, 290(1). doi: 10.1016/j.ydbio.2005.11.009.

White, K. A. *et al.* (2017) 'Cancer-associated arginine-to-histidine mutations confer a gain in pH sensing to mutant proteins.', *Science signaling*. American Association for the Advancement of Science, 10(495). doi: 10.1126/scisignal.aam9931.

White, K. A., Grillo-Hill, B. K. and Barber, D. L. (2017) 'Cancer cell behaviors mediated by dysregulated pH dynamics at a glance.', *Journal of cell science*. The Company of Biologists Ltd, 130(4), pp. 663–669. doi: 10.1242/jcs.195297.

White, K. A., Kisor, K. and Barber, D. L. (2019) 'Intracellular pH dynamics and charge-changing somatic mutations in cancer', *Cancer and Metastasis Reviews*. Cancer Metastasis Rev, pp. 17–24. doi: 10.1007/s10555-019-09791-8.

Xu, J. *et al.* (2020) 'Ca9 silencing promotes mitochondrial biogenesis, increases putrescine toxicity and decreases cell motility to suppress ccrcc progression', *International Journal of Molecular Sciences*, 21(16). doi: 10.3390/ijms21165939.

Yuan, X. *et al.* (2015) 'Expression of Notch1 correlates with breast cancer progression and prognosis', *PLoS ONE*, 10(6). doi: 10.1371/journal.pone.0131689.

Zerbino, D. R. *et al.* (2018) 'Ensembl 2018', *Nucleic Acids Research*. doi: 10.1093/nar/gkx1098.

Zhao, H. *et al.* (2019) ‘Dynamic imaging of cellular pH and redox homeostasis with a genetically encoded dual-functional biosensor, pHaROS, in yeast’, *Journal of Biological Chemistry*, 294(43). doi: 10.1074/jbc.RA119.007557.

Zhou, W. *et al.* (2012) ‘HIF1α induced switch from bivalent to exclusively glycolytic metabolism during ESC-to-EpiSC/hESC transition’, *EMBO Journal*, 31(9). doi: 10.1038/emboj.2012.71.